A Direct Ab Initio Dynamics Study of the Water-Assisted Tautomerization of Formamide

ROBERT L. BELL, DENI L. TAVERAS, THANH N. TRUONG, JACK SIMONS

Department of Chemistry, University of Utah, Salt Lake City, Utah 84112

Received 24 January 1996; revised 6 November 1996; accepted 7 November 1996

ABSTRACT: Direct ab initio dynamics calculations based on a canonical variational transition-state theory with several multidimensional semiclassical tunneling approximations were carried out to obtain rate constants for the water-assisted tautomerization of formamide. The accuracy of the density functionals, namely, B-LYP, B3-LYP, and BH&H-LYP, were examined. We found that the BH&H-LYP method yields the most accurate transition-state properties when comparing it to ab initio MP2 and QCISD results, whereas B-LYP and B3-LYP methods predict barrier heights too low. Reaction path information was calculated at both the MP2 and nonlocal hybrid BH&H-LYP levels using the 6-31G(d,p) basis set. At the BH&H-LYP level, we found that the zero-point energy motion lowers the barrier to tautomerization in the formamide–water complex by 3.6 kcal/mol. When tunneling is considered, the activation energy at the BH&H-LYP level at 300 K is 17.1 kcal/mol. This is 3.4 kcal/mol below the zero-point-corrected barrier and 7.0 kcal/mol below the classical barrier. Excellent agreement between BH&H-LYP and MP2 rate constants further supports the use of BH&H-LYP for rate calculations of large systems. Int J Quant Chem **63**: 861–874, 1997

Introduction

Proton-transfer reactions are important in many chemical and biological systems [1–3]. A particularly interesting type of proton transfer in aqueous solution is one in which one or more solvent water molecules can mediate the process by serving as a bridge that connects the donor and acceptor sites. These water molecules stabilize the transition state and therefore substantially lower the classical energy barrier to proton transfer. Such phenomena have been postulated in the action of enzymes (e.g., carbonic anhydrase [4]) as well as in other tautomerization reactions [5, 6]. In this study, we examined the water-assisted tautomerization of formamide to formamidic acid. This class of reac-

Correspondence to: T. N. Truong.
Contract grant sponsor: University of Utah.
Contract grant sponsor: National Science Foundation.
Contract grant number: 9116286.

 CCC 0020-7608 / 97 / 040861-14

tions has importance in protein and pharmaceutical chemistry and provides the simplest model for peptide linkage [5, 7–17]. The NCO backbone of formamide is also found in DNA bases, particularly in guanine, cytosine, and thymine. Therefore, formamide can serve as a model for tautomerization in these bases.

Several theoretical studies on the monohydrated formamide–water complex have determined that the preferred mechanism to form formamidic acid proceeds via a stable cyclic double hydrogen-bonded transition state [10, 11, 14, 18–21]. In a previous study (hereinafter referred to as article I) by Wang et al. [14], it was found that the tautomerization of formamide to formamidic acid [see Fig. 1(a)] has a classical barrier of 52 kcal/mol in the gas phase. A single water molecule directly assists the tautomerization of formamide by acting as a bridge for proton transfer from the donor (—NH) to the acceptor (=O) site [see Fig. 1(b)] and, consequently, lowers the barrier to 26 kcal/mol. Furthermore, it was determined that this water-assisted tautomerization proceeds via a *concerted* double proton-transfer mechanism. Structural and frequency information at the stationary points were also presented in article I. A dynamical study on the similar water-assisted tautomerization of formamidine [6, 22] found that both the zero-point energy (ZPE) and tunneling corrections greatly affected the rate of reaction. One can expect similar results for the water-assisted tautomerization of formamide; however, a quantitative dynamical study for this system has not been done and is a principal part of this study.

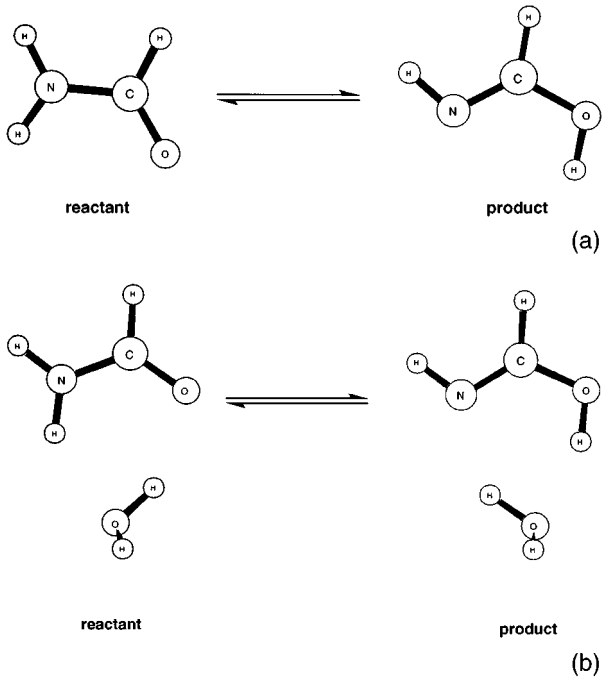

FIGURE 1. (a) Formamide gas-phase tautomerization. (b) Formamide water-assisted tautomerization.

The present work has two purposes: (i) to continue the efforts of article I by carrying out accurate thermal rate calculations for the forward and reverse reactions of the water-assisted tautomerization of formamide with special attention given to quantal effects, namely, tunneling and zero-point energy motion; and (ii) because use of density functional theory (DFT) can significantly reduce the computational demand for rate calculations [23], we test the accuracy of density functional theory (DFT) [6, 22, 23] for studying reactions of this type. Comparisons are made between ab initio, namely, MP2 and QCISD, and DFT methods. The DFT methods utilized are Becke's (B), the hybrid Becke's half-and-half method (BH&H), and Becke's three-parameter (B3) for exchange energy in combination with the Lee–Yang–Parr (LYP) functional for correlation energy. A smaller number of electronic structure calculations were also performed for the gas-phase reaction for comparison purposes.

To obtain kinetics information, a conventional dynamical approach [24] cannot be employed here since an analytical potential energy function does not exist. An alternative is to utilize our direct ab initio dynamics approach [25], although other direct dynamics approaches such as those discussed in a recent review [26] can also be used. The direct ab initio dynamics approach utilized here is based on a variational transition-state theory (VTST) augmented with multidimensional semiclassical tunneling corrections. In this case, geometry, energy, gradient, and Hessian information along the minimum energy path (MEP) is calculated directly from molecular orbital and density functional theory. Below, we provide a brief overview of variational transition-state theory, followed by computational details, results and discussion, and summary sections.

Variational Transition-State Theory

The canonical variational transition-state (CVT) rate constant for a given temperature is obtained

by varying the location of the dividing surface along the MEP, which intersects and is orthogonal to the MEP, so as to minimize the number of recrossings trajectories [27–29]. The reaction coordinate s is defined as the distance along the MEP with the origin at the transition state with positive direction toward the product and negative direction toward the reactant. The generalized transition state and reactant partition functions can be written as products of the individual electronic, rotational, and vibrational partition functions, with the assumption that all degrees of freedom are separable. The electronic partition functions for both the generalized transition state and reactant are assumed to cancel. The rotational partition functions were calculated by classical formulation due to small energy spacing. The vibrational partition functions are treated quantum mechanically within the local harmonic approximation. Note that the CVT rate theory still treats the reaction coordinate classically. To include quantal effects, i.e., tunneling, along the reaction coordinate, the rate constant is multiplied by the ground-state transmission coefficient [27–29].

Tunneling Methods

The ground-state transmission coefficient used here is defined as the ratio of the thermally averaged multidimensional semiclassical ground-state transmission probability to the thermally averaged classical transmission probability for tunneling through an effective potential which is approximated to be the vibrational adiabatic ground-state potential curve.

Four approximations for tunneling were used: At the transition state theory (TST) level of rate calculation, where potential energy information is only available at the stationary points, the Wigner [30] and zero-curvature tunneling at zeroth-order interpolation denoted as ZCT-0 [31] are used. The ZCT-0 approximation is commonly known as Eckart tunneling. The Wigner tunneling correction assumes that most of the tunneling occurs at the top of the barrier and is only reasonable at moderate to high temperatures. The ZCT-0 tunneling correction has been found to be more accurate than the Wigner tunneling probabilities due to the use of a one-dimensional Eckart potential curve fitted to the reaction enthalpy at 0 K, zero-point-corrected barrier height, and curvature near the transition state. Note that the zero-curvature and the centrifugal-dominant small-curvature semiclassical adiabatic ground-state (CD-SCSAG) approximations are both multidimensional and are used with CVT rate calculations. For brevity, the zero and small-curvature tunneling cases are labeled ZCT and SCT, respectively. The zero-curvature approximation assumes that the tunneling path follows the MEP. The SCT tunneling approximation includes ''corner-cutting'' effects by assuming the tunneling path to follow the vibrational turning points in the direction of the internal-centri-

TABLE I
Calculated frequencies (cm^{-1}) of formamide.

	Reactant			Transition state			Product		
Expt.[a]	BH&H-LYP	B3-LYP	MP2	BH&H-LYP	B3-LYP	MP2	BH&H-LYP	B3-LYP	MP2
289	206.5	149.6	104.4	2117.0i	1912.8i	1972.3i	615.0	589.7	588.8
581	588.1	563.0	564.7	490.7	457.5	439.7	651.0	644.8	643.0
603	663.5	647.3	649.4	916.6	872.7	877.2	870.8	832.2	848.7
1021	1104.1	1047.0	1058.3	1099.7	1031.3	1038.0	1117.3	1054.2	1063.8
1046	1108.0	1054.7	1073.5	1161.1	1112.8	1127.5	1127.5	1081.4	1092.8
1258	1329.5	1275.9	1304.5	1206.1	1165.3	1187.1	1251.5	1200.8	1207.6
1390	1489.7	1433.7	1459.0	1280.7	1233.5	1267.7	1432.4	1384.6	1398.8
1577	1687.6	1621.1	1657.8	1534.9	1456.6	1471.6	1479.3	1414.7	1431.4
1758	1922.5	1836.5	1841.9	1729.0	1659.3	1696.1	1841.5	1750.7	1752.2
2854	3082.7	2953.1	3067.5	2260.1	2143.2	2186.1	3229.9	3117.7	3221.1
3439	3729.9	3594.4	3690.9	3276.9	3174.1	3268.7	3669.3	3520.2	3613.3
3563	3876.1	3738.8	3844.8	3745.0	3581.7	3682.9	3932.0	3739.5	3807.7

[a] [37].

fugal force [28, 32]. Thus, the CVT/SCT level represents the most accurate dynamical treatment. Detailed discussions of both the ZCT and SCT tunneling approximations are given elsewhere [27–29].

Electronic Structure Calculations

Geometries of the reactant, transition state, and product for the tautomerization in the formamide–water complex were calculated at the MP2 and quadratic configuration interaction, including single and double excitations (QCISD), levels of theory and also with B-LYP, B3-LYP, and BH&H-LYP DFT methods. Note that the BH&H-LYP functional as implemented in the G92/DFT [33] is given by

$$E_{XC} = 0.5E_X^{HF} + 0.5E_X^{Slater} + E_C^{LYP}, \qquad (1)$$

where E_X^{HF} and E_X^{Slater} are the Hartree–Fock and Slater exchange energies, respectively, and E_C^{LYP} is the LYP correlation energy. The double-zeta plus polarization 6-31G(d,p) basis set was used in all the calculations. The MEP at the BH&H-LYP level was calculated with a step size of 0.1 amu$^{1/2}$bohr for a total of 20 steps in each direction from the transition state. The MEP at the MP2 level was calculated with a step size of 0.05 amu$^{1/2}$bohr for a total of 40 steps in each direction from the transition state. Hessian calculations were performed at the MP2 and BH&H-LYP levels at selected points along the MEP. All the electronic structure calculations were done using the G92/DFT and G94 [34] programs.

Rate Calculations

An automated focusing technique [35] was used to choose a set of 21 points, including the transition state, along the BH&H-LYP and MP2 MEPs for which Hessian calculations were carried out. The focusing technique was designed to minimize the number of Hessian points on the MEP while maintaining a reasonable level of accuracy. From our experience, rate constants with appreciable tunneling contributions require at least 21 Hessian points. To check the convergence, we also performed a 30-Hessian point—points chosen by the same focusing technique—rate calculation, at the

TABLE II
Calculated frequencies (cm^{-1}) of the formamide–water system.

Reactant			Transition state			Product		
BH&LH-LYP	B3-LYP	MP2	BH&LH-LYP	B3-LYP	MP2	BH&H-LYP	B3-LYP	MP2
161.3	159.8	144.9	1768.8i	1539.4i	1653.0i	196.2	196.3	188.7
204.8	204.9	191.3	282.7	266.0	267.7	230.2	230.8	216.1
214.9	215.4	205.3	525.5	518.0	524.8	249.9	260.4	244.5
262.9	264.2	251.5	583.6	558.0	567.1	346.8	368.6	340.5
371.3	365.8	354.9	603.8	571.3	590.1	402.6	402.9	385.8
451.8	441.3	424.6	650.1	605.7	623.3	686.6	668.6	658.9
643.6	624.2	616.9	716.7	687.3	708.1	818.7	806.9	793.3
760.8	783.1	745.8	854.6	824.5	825.4	845.7	854.6	832.4
838.7	836.2	815.4	1110.9	1040.1	1053.6	956.5	965.3	943.7
1115.7	1053.3	1070.0	1119.0	1112.9	1125.8	1129.1	1075.6	1086.9
1145.5	1100.4	1111.8	1284.0	1320.8	1336.2	1167.1	1124.6	1131.0
1391.4	1344.3	1364.9	1410.9	1361.4	1389.8	1352.4	1307.5	1312.6
1486.1	1427.7	1454.9	1445.3	1417.1	1444.0	1492.0	1427.1	1445.4
1694.9	1622.8	1659.4	1535.5	1474.4	1508.1	1547.1	1512.8	1515.9
1740.3	1696.2	1717.5	1555.2	1517.1	1561.1	1730.2	1685.3	1706.4
1881.9	1795.9	1820.6	1720.4	1647.8	1676.6	1816.9	1727.8	1743.8
3110.9	2993.6	3096.8	1832.9	1748.2	1784.8	3222.4	3109.3	3210.9
3596.0	3415.7	3566.7	2042.3	1962.0	1994.6	3532.5	3220.7	3422.1
3793.3	3577.9	3721.6	3197.3	3088.3	3185.7	3685.6	3457.2	3621.2
3842.9	3701.0	3810.1	3761.7	3613.7	3704.9	3719.5	3536.8	3649.4
4044.9	3864.5	3966.7	4010.7	3829.9	3903.4	4037.6	3857.2	3953.5

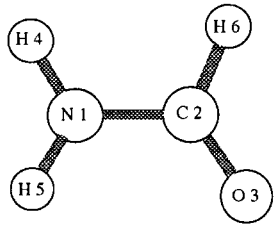

Reactant

		Deviation from experiment		
Variables	Experiment	MP2	BH&H-LYP	B3-LYP
N1C2	1.352	0.010	-0.002	0.009
C2O3	1.219	0.005	-0.016	-0.003
N1H4	1.002	0.001	-0.005	0.005
N1H5	1.002	0.004	-0.002	0.007
C2H6	1.098	0.003	0.000	0.011
N1C2O3	124.7	0.1	0.3	0.2
C2N1H4	120.0	1.4	1.7	1.7
C2N1H5	118.5	0.1	0.4	0.5
N1C2H6	112.7	-0.6	-0.3	-0.7

(a)

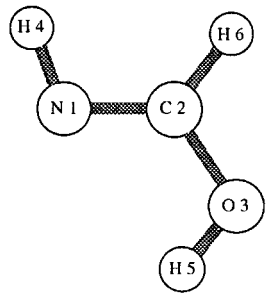

Product

		Deviation from MP2	
Variables	MP2	BH&H-LYP	B3-LYP
N1C2	1.274	-0.020	-0.007
C2O3	1.350	-0.017	-0.004
N1H4	1.016	-0.008	-0.003
N1H5	2.294	-0.006	0.000
C2H6	1.088	-0.003	0.006
N1C2O3	121.6	0.7	0.5
C2N1H4	110.0	1.3	0.8
C2N1H5	54.4	-0.2	0.0
N1C2H6	128.1	-0.8	-0.1

(b)

FIGURE 2. (a) Optimized structural data of the gas-phase formamide (reactant) at the MP2, B3-LYP, and BH&H-LYP / 6-31G(d,p) levels of theory with experimental data. Bond lengths are in angstroms and angles are in degrees. Experimental values are taken from [14]. (b) Similar to (a) except for product structure. (c) Similar to (a) except for transition-state structure.

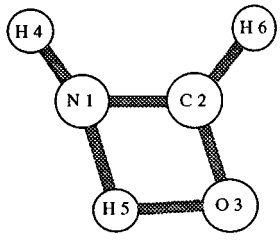

Transition State

Variables	MP2	Deviation from MP2 BH&H-LYP	Deviation from MP2 B3-LYP
N1C2	1.274	-0.016	-0.004
C2O3	1.350	-0.019	-0.005
N1H4	1.016	-0.008	0.004
N1H5	2.294	-0.003	0.015
C2H6	1.088	-0.003	0.006
N1C2O3	121.6	-0.3	0.0
C2N1H4	110.0	0.4	-0.2
C2N1H5	105.4	0.2	0.3
N1C2H6	128.1	0.1	0.1

(c)

FIGURE 2. (Continued).

MP2 level. We found that at 300 K the CVT/SCT rate constants converged to within 1.7% for the forward rate. This is a very acceptable level of accuracy given that experimental uncertainty is often larger than 20%.

The classical potential energy barrier for the MP2 and BH&H-LYP rate calculations were scaled factors of 1.151 and 1.075, respectively, to reproduce the more accurate QCISD barrier. TheRate (theoretical rate) [36] program was used to carry out all TST and CVT rate and tunneling calculations.

Geometries and Frequencies

Although the structures and frequencies of the equilibrium structures were discussed in detail in article I at the Hartree–Fock level, we have included the formamide and formamide–water frequencies of the equilibrium structures at the BH&H-LYP, B3-LYP, MP2, and QCISD levels of theory and experiment in Tables I and II, respectively. The equilibrium geometries of formamide are of C_s symmetry for both DFT methods. At the MP2 level, the equilibrium structure was found to be of C_1 symmetry. These were determined from frequency calculations which yielded all real frequencies for all methods. Below, we will focus our attention on the accuracy of the DFT methods.

Specifically for the equilibrium structures found in Figures 2(a) and (b) and 3(a) and (b), the B3-LYP, BH&H-LYP, and MP2 structural data are in overall very good agreement with the highest level of theory or available experimental data. The MP2 method is, in general, better than both of the DFT methods with the largest difference of 0.059 Å for bond lengths and of 1.4° for angles. As for the BH&H-LYP and B3-LYP methods, their results compared equally well with the MP2 and QCISD results. In particular, differences for bond lengths range from 0.077 to 0.119 Å and from 2.7 to 3.2° for angles for the BH&H-LYP and B3-LYP methods, respectively. However for the hydrogen-bonded complexes [see Fig. 3(a) and (b)], both DFT methods tend to slightly underestimate bond lengths, although the BH&H-LYP method yields better results for active bonds, bonds which are either being formed and broken in the course of the reaction.

To get an idea of the reliability of frequency calculations, the averaged unsigned percent differ-

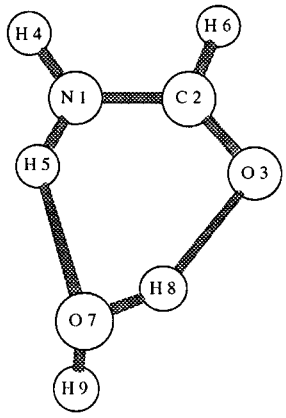

Reactant

Variables	QCISD	Deviation from QCISD MP2	BH&H-LYP	B3-LYP
N1C2	1.351	-0.002	-0.014	-0.003
N1H4	1.003	0.000	-0.006	0.004
N1H5	1.013	0.002	-0.003	0.009
C2O3	1.232	0.004	-0.017	-0.002
C2H6	1.099	0.000	-0.004	0.006
O3H8	1.973	-0.030	-0.058	-0.064
H5O7	2.055	-0.038	-0.057	-0.079
O7H8	0.971	0.003	-0.005	0.009
O7H9	0.962	0.000	-0.009	0.004
N1C2H6	113.6	0.0	0.2	0.2
N1C2O3	124.9	0.0	0.0	-0.1
N1H5O7	140.5	0.2	-0.5	0.4
C2N1H4	120.6	0.1	0.3	0.3
C2N1H5	118.3	-0.3	-0.3	-0.8
C2O3H8	106.1	-0.6	0.2	-0.6
H5O7H8	79.2	0.2	1.1	0.6
H9O7H5	115.1	-0.4	2.5	-3.2
H9O7H8	104.2	-0.2	1.0	-0.3

FIGURE 3. (a) Optimized structural data of the formamide–water complex (reactant) at the MP2, BH&H-LYP, B3-LYP, and QCISD / 6-31G(d, p) levels of theory. Bond lengths are in angstroms and angles are in degrees. (b) Similar to (a) except for product structure. (c) Similar to (a) except for transition-state structure.

ences between experimental [37], BH&H-LYP, B3-LYP, and MP2 methods for all harmonic frequencies for the formamide structure were calculated. As can be seen in Table I, BH&H-LYP, B3-LYP, and MP2 methods overestimate the experimental values, except for the lowest two, by unsigned averages of 9.0, 7.2, and 10.2%, respectively.

The average unsigned percent difference between the MP2, B3-LYP, and BH&H-LYP methods for all frequencies for the formamide–water equilibrium structures were calculated. For these structures, both DFT method overestimate the vibrational frequencies when compared to the MP2 method by unsigned averages of 3.1 and 3.2% for the BH&H-LYP and B3-LYP methods, respectively.

For the transition-state structures [see Figs. 2(c) and 3(c)], specifically for the gas-phase system, DFT results are very close to the MP2 ones. The largest deviations range from 0.019 to 0.015 Å for bond lengths and from 0.4 to 0.3° for angles for the BH&H-LYP and B3-LYP methods, respectively. For the hydrogen-bonded complex, all three methods are comparable. The MP2 method displays the

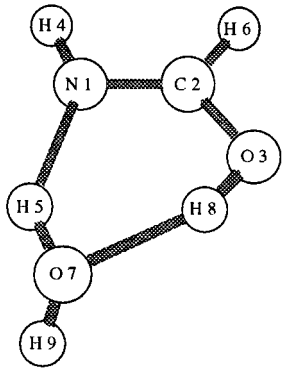

Product

Variables	QCISD	Deviation from QCISD MP2	BH&H-LYP	B3-LYP
N1C2	1.280	0.004	-0.015	0.000
N1H4	1.015	0.000	-0.008	0.002
N1H5	2.013	-0.059	-0.077	-0.119
C2O3	1.337	-0.003	-0.021	-0.010
C2H6	1.089	-0.001	-0.004	0.005
O3H8	0.974	0.016	0.004	0.024
H5O7	0.962	0.014	0.008	0.025
O7H8	1.830	-0.053	0.060	-0.091
O7H9	0.962	0.001	-0.008	0.004
N1C2H6	125.5	0.0	-0.5	-0.3
N1C2O3	123.4	-0.1	0.2	0.0
N1H5O7	140.1	0.6	0.9	2.1
C2N1H4	110.2	-0.1	1.3	1.1
C2N1H5	106.0	-0.3	-0.5	-0.7
C2O3H8	108.1	-0.5	0.9	-0.2
H5O7H8	82.4	0.7	1.0	0.5
H9O7H5	104.6	-0.1	1.2	0.0
H9O7H8	111.2	0.1	2.7	-1.2

FIGURE 3. (Continued).

largest deviations of 0.034 Å for bond lengths and of 0.8° for angles. Both the BH&H-LYP and B3-LYP methods yield deviations in bond lengths on the order of 0.03 Å and of 1.5° for angles.

Average unsigned percent differences between the MP2, B3-LYP, and BH&H-LYP methods for all frequencies for the formamide–water transition state yield different results. The BH&H-LYP method gives frequencies that are 2.5% greater than the MP2 frequencies while the B3-LYP method gives frequencies smaller by 2.1%. All methods yielded a single imaginary frequency for the transition state. The MP2 method gave a frequency of 1653i cm^{-1}, the BH&H-LYP method gave one of 1769i cm^{-1}, and the B3-LYP method gave one of 1539i cm^{-1}.

Energetics

The reaction energetics for both the gas-phase and water-assisted tautomerizations as well as the energetics for the formation of these complexes are given in Table III. The energetics of formation of the formamide–water and formamidic–water

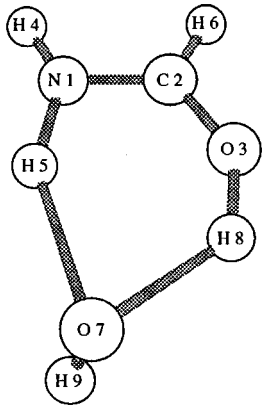

Transition State

		Deviation from QCISD		
Variables	QCISD	MP2	BH&H-LYP	B3-LYP
N1C2	1.310	0.001	-0.014	-0.002
N1H4	1.008	0.001	-0.007	0.004
N1H5	1.300	0.009	-0.001	0.018
C2O3	1.288	0.001	-0.018	-0.004
C2H6	1.091	0.000	-0.003	0.006
O3H8	1.190	0.034	-0.018	0.029
H5O7	1.190	-0.006	-0.007	0.002
O7H8	1.208	0.002	-0.003	0.019
O7H9	0.964	0.002	-0.009	0.003
N1C2H6	121.3	0.0	-0.1	0.0
N1C2O3	121.8	0.2	0.2	0.3
N1H5O7	148.3	0.1	-0.3	-0.1
C2N1H4	116.4	-0.4	0.6	0.2
C2N1H5	105.2	-0.1	-0.1	0.0
C2O3H8	102.7	-0.3	0.8	0.5
H5O7H8	84.8	-0.1	0.1	-0.2
H9O7H5	110.0	-0.8	1.4	-0.9
H9O7H8	109.7	-0.7	1.5	-0.5

FIGURE 3. (Continued).

complexes favor the BH&H-LYP method when comparisons are made to the MP2 results for both the change in total energy, ΔE, and the reaction enthalpy at 0 K, ΔH_0^0. As found in article I , the classical barrier for the tautomerization in the gas phase is 51.9 kcal/mol at CISD(FULL) using the Dunning correlation consistent polarized valence double-zeta plus basis set [38]. This barrier is lowered to 26.0 kcal/mol when a single water molecule is added. Zero-point energy corrections lower these barriers by 3.0 and 3.4 kcal/mol for the gas-phase and monohydrated cases, respectively.

The BH&H-LYP/6-31G(d,p) gas-phase classical barrier of 51.8 kcal/mol is nearly equal to the CISD(FULL) barrier. Both the MP2 and B3-LYP classical barriers are approximately 5 kcal/mol and the B-LYP is over 9 kcal/mol below the BH&H-LYP and CISD(FULL) barriers. The BH&H-LYP water-assisted classical barrier of 24.1 kcal/mol gives the best agreement with the QCISD barrier of 25.9 kcal/mol when compared with the MP2, B3-LYP, and B-LYP barriers of 22.5, 19.5, and 16.9 kcal/mol, respectively. The BH&H-LYP method also gives the best zero-point-corrected

TABLE III
Reaction energetics for the formamide gas-phase and water-assisted tautomerizations; all energies in kcal / mol.

	ΔE	ΔH_0^0	$\Delta V^{\ddagger}$	$\Delta V_a^{\ddagger G}$
$F + H_2O \rightarrow F(H_2O)$				
B-LYP	−13.7	−10.6		
B3-LYP	−13.5	−10.3		
BH&H-LYP	−13.2	−10.1		
MP2[a]	−12.8	−9.7		
$FA + H_2O \rightarrow FA(H_2O)$				
B-LYP	−16.5	−13.6		
B3-LYP	−16.0	−13.0		
BH&H-LYP	−15.3	−12.2		
MP2[a]	−14.7	−11.7		
$F \rightarrow FA$				
B-LYP	12.6	13.1	42.4	39.4
B3-LYP	12.6	13.2	46.2	43.3
BH&H-LYP	12.6	13.2	51.8	48.8
MP2[a]	12.3	12.8	46.8	43.8
CISD(FULL)[a]	11.4		51.9	48.9
$F(H_2O) \rightarrow FA(H_2O)$				
B-LYP	9.8	10.1	16.9	13.7
B3-LYP	10.1	10.6	19.5	16.2
BH&LYP	10.5	11.0	24.1	20.5
MP2[a]	10.5	10.9	22.5	19.2
QCISD	10.5		25.9	
CISD(FULL)[a]	10.9		26.0	22.6

[a][14].

barriers with differences from the CISD results being 0.1 and 2.1 kcal/mol for the gas-phase and monohydrated systems, respectively.

Minimum-Energy Path

The potential energy along with the corresponding structural changes in the formamide–water complex along the MEP are illustrated in Figures 4 and 5, respectively. This system reveals a concerted two-stage mechanism in qualitative agreement with that for the formamidine–water system [6]. From an examination of the structural changes from reactant to product, it can be seen that the NCO bond angle undergoes compression first, then the NH bond starts to lengthen. Specifically, tautomerization in the formamide–water system requires the NCO bond angle to be compressed by only 2.9° or 2.3% from the equilibrium value then the NH bond is stretched from an equilibrium value of 1.010–1.299 Å at the transition state, an increase of 28%.

For tautomerization to occur, the formamide (gas-phase) molecule must undergo large structural changes that are energetically expensive. The NCO bond angle is compressed from an equilibrium value of 124.8° to 108.6°, a 13% decrease. The NH bond is then stretched from 1.006 to 1.320 Å, an increase of 31%, to reach the transition state. The large reduction in the classical energy barrier from the gas phase to the water-assisted case is attributed to the water acting as a catalyst through the stabilization of the transition state [4–6, 14, 18, 19, 22]. Most of the energy savings is achieved because the NCO angle has to be compressed by only 2.9° when compared with that for the gas phase which has to be compressed by 16.7°.

The BH&H-LYP and MP2 generalized frequencies ($> 500\ cm^{-1}$) in Figure 6 show similar results, consistent with the results for the stationary points. In a previous study on the $CH_4 + H$ reaction by Truong and Duncan [39], it was shown in a plot

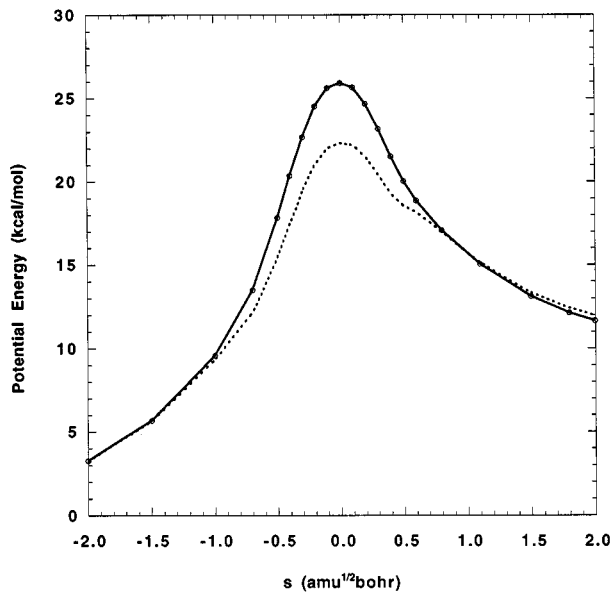

FIGURE 4. Classical, V_{MEP} (solid), and zero-point corrected, V_a^G (dotted), potential energy vs. reaction coordinate for the water-assisted formamide tautomerization at the BH&H-LYP / 6-31G(*d*,*p*) level. Circles indicate where Hessians are also available.

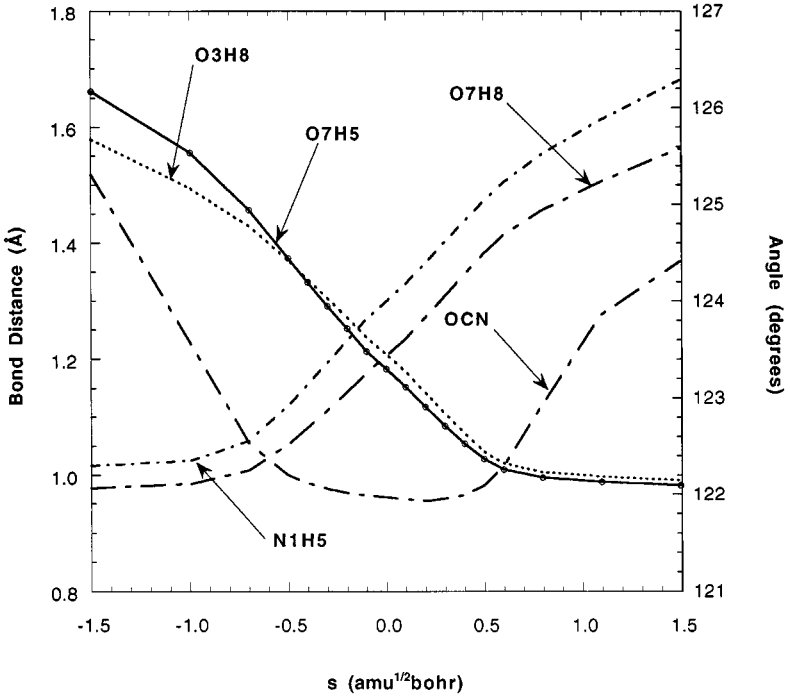

FIGURE 5. Geometric parameters vs. reaction coordinate for the water-assisted formamide tautomerization at the BH&H-LYP / 6-31G(d, p) level. The reader is referred to Figures 3(a)–(c) for definitions of bond distances.

similar to Figure 6 that generalized transition-state frequencies calculated at the BH&H-LYP/6-311G(d, p) were found to be in excellent agreement with the QCISD/6-311G(d, p) results.

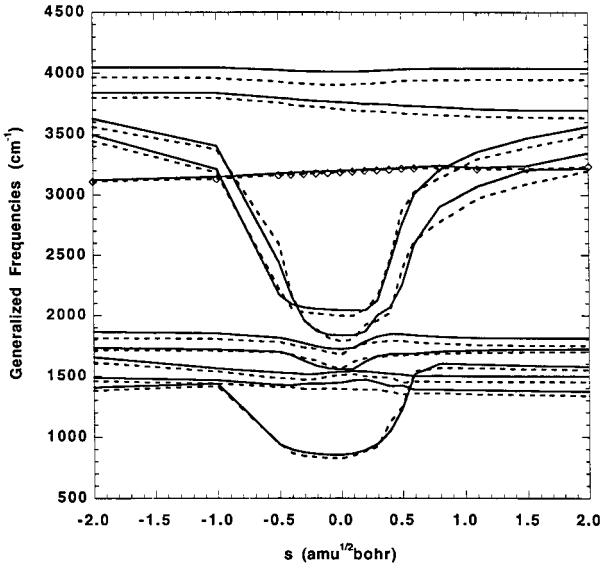

FIGURE 6. Plot of the (solid) BH&H-LYP and (dashed) MP2 generalized frequencies ($\geq$ 500 cm^{-1}) vs. reaction coordinate. Diamonds indicate where Hessians are available.

Rate Constants

The following discussion will focus on the forward reaction, also being qualitatively representative of the reverse. The canonical rate constants for the formamide water-assisted tautomerizations for both the forward and reverse reactions are given in Tables IV and V, respectively. The data given in Tables IV and V are displayed graphically in Figures 7 and 8.

The difference between the TST and CVT rate constants reveal the importance of the recrossing effect. In particular, at 300 K, the CVT rate is smaller by a factor of 1.01, indicating that such effects are small.

As tunneling is included, Figure 7 shows increasing non-Arrhenius behavior with increasing accuracy in the level of tunneling approximations. The largest deviation from Arrhenius behavior can be observed in the CVT/SCT rate constants. A comparison of the Wigner rate constant, denoted as TST/W, with the TST/ZCT-0 rate constant, at 300 K, shows that the latter rate constant is larger by a factor of 374 for reasons discussed in the tunneling section. Another effect of the barrier

TABLE IV
Rate constants (s^{-1}) for the formamide water-assisted forward reaction at the BH&H-LYP / 6-31G(*d*, *p*) level.

T / K	TST	TST / W	TST / ZCT-0	CVT	CVT / ZCT	CVT / SCT	CVT / SCT (MP2)[a]
200	4.58E − 13	3.55E − 12	8.17E − 10	4.49E − 13	3.59E − 11	8.40E − 8	5.93E − 7
250	3.02E − 8	1.61E − 7	2.27E − 6	2.97E − 8	3.19E − 7	2.71E − 6	7.65E − 6
300	4.67E − 5	1.87E − 4	7.00E − 4	4.61E − 5	2.07E − 4	4.61E − 4	7.70E − 4
350	8.55E − 3	2.74E − 2	5.31E − 2	8.47E − 3	2.40E − 2	3.46E − 2	4.53E − 2
400	4.17E − 1	1.12	1.52	4.13E − 1	8.94E − 1	1.08	1.21
450	8.45	1.97E + 1	2.18E + 1	8.38	1.52E + 1	1.70E + 1	1.72E + 1
500	9.31E + 1	1.93E + 2	1.89E + 2	9.24E + 1	1.48E + 2	1.60E + 2	1.49E + 2
600	3.37E + 3	5.89E + 3	4.93E + 3	3.34E + 3	4.62E + 3	4.78E + 3	4.10E + 3
800	2.98E + 5	4.24E + 5	3.11E + 5	2.96E + 5	3.54E + 5	3.58E + 5	2.83E + 5
1000	4.47E + 6	5.68E + 6	3.92E + 6	4.45E + 6	4.97E + 6	5.01E + 6	3.80E + 6

[a]30 Hessian point rate constant.

shape is shown in the difference between the TST/ZCT-0 and CVT/ZCT rate constants. At 300 K, the CVT/ZCT rate constant is smaller by a factor of 2.21. This is because the Eckart potential often has a too narrow width. The effect of ''corner cutting'' can be seen in a comparison of the CVT/ZCT and CVT/SCT rate constants. At 300 K, the CVT/SCT rate constant is larger by a factor of 2.23. The 30-Hessian point CVT/SCT rate constant at the MP2 level is larger than the BH&H-LYP counterpart by a factor of 1.67 at 300 K for the forward rate. Recall that both the BH&H-LYP and MP2 potential curves were scaled to yield the QCISD barrier.

Tunneling effects can be reflected through the strong temperature dependence of the activation energy, E_a, which is the slope of Arrhenius curves (see Table VI). At the most accurate level of rate theory considered here, namely, the CVT/SCT level, the activation energy decreases from 20.7 to 13.5 kcal/mol as the temperature decreases from 800 to 200 K. At 300 K, the calculated activation energy is 17.1 kcal/mol. This is 3.4 kcal/mol below the zero-point corrected barrier and 7.0 kcal/mol below the classical barrier.

Summary

We carried out direct ab initio and DFT dynamics calculations on the water-assisted tautomerization of formamide to obtain canonical rate constants and found many similarities with the water-assisted tautomerization of formamidine [6].

TABLE V
Rate constants (s^{-1}) for the formamide water-assisted reverse reaction at the BH&H-LYP / 6-31G(*d*, *p*) level.

T / K	TST	TST / W	TST / ZCT-0	CVT	CVT / ZCT	CVT / SCT	CVT / SCT (MP2)[a]
200	9.00E − 1	6.98	1.61E + 3	8.84E − 1	7.06E + 1	7.38E + 3	2.24E + 4
250	2.49E + 2	1.33E + 3	1.88E + 4	2.46E + 2	2.64E + 3	2.24E + 4	4.45E + 4
300	1.03E + 4	4.13E + 4	1.55E + 5	1.02E + 4	4.57E + 4	1.02E + 5	1.31E + 5
350	1.45E + 5	4.64E + 5	9.00E + 5	1.43E + 5	4.07E + 5	5.86E + 5	6.27E + 5
400	1.04E + 6	2.80E + 6	3.80E + 6	1.03E + 6	2.23E + 6	2.70E + 6	2.59E + 6
450	4.80E + 6	1.12E + 7	1.24E + 7	4.76E + 6	8.63E + 6	9.66E + 6	8.65E + 6
500	1.62E + 7	3.38E + 7	3.27E + 7	1.61E + 7	2.59E + 7	2.78E + 7	2.39E + 7
600	1.01E + 8	1.77E + 8	1.48E + 8	1.00E + 8	1.38E + 8	1.43E + 8	1.17E + 8
800	1.00E + 9	1.43E + 9	1.05E + 9	9.97E + 8	1.19E + 9	1.21E + 9	9.59E + 8
1000	4.09E + 9	5.19E + 9	3.58E + 9	4.06E + 9	4.54E + 9	4.58E + 9	3.61E + 9

[a]30 Hessian point rate constant.

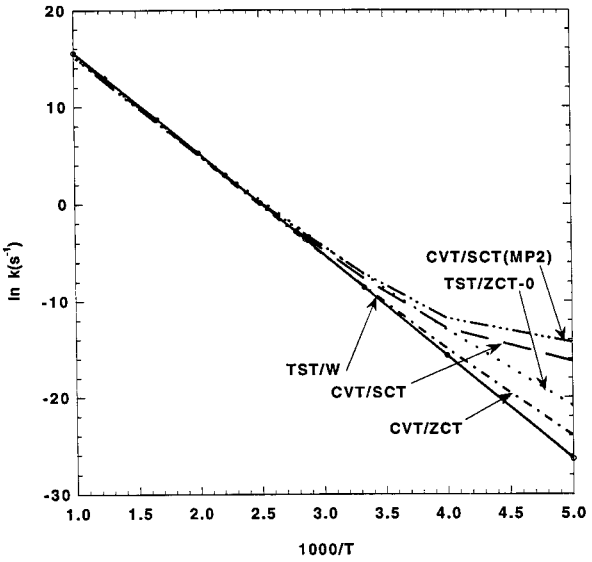

FIGURE 7. Arrhenius plot of (solid) TST / W, (dotted) TST / ZCT-0, (dash-dotted) CVT / ZCT, and (long-dashed) CVT / SCT calculated at the BH&H-LYP / 6-31G(d, p) level and (long dash, three dots) CVT / SCT rate constants calculated at the MP2 / 6-31G(d, p) level using 30 Hessian points vs. 1000 / T (K) for the formamide–water complex forward reaction. Both the BH&H-LYP and MP2 potential barriers were scaled to match the QCISD barrier.

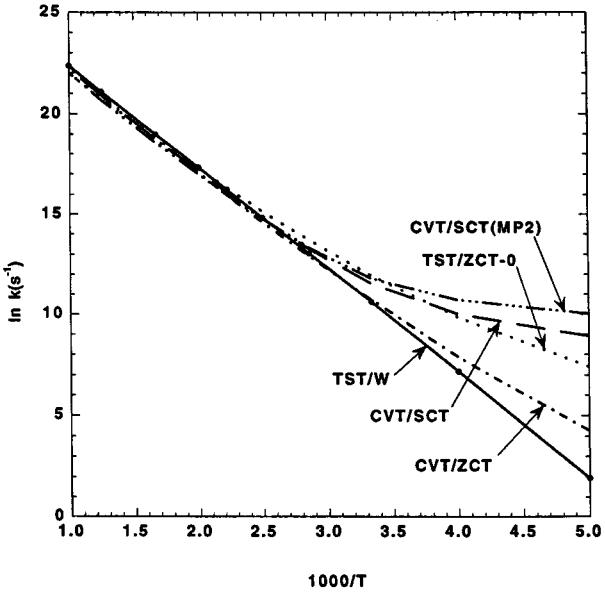

FIGURE 8. Similar to Figure 7 except for the reverse reaction.

TABLE VI

Activation energies (kcal / mol) of the formamide–water tautomerization for the forward and reverse directions calculated at the BH&LH-LYP / 6-31G(d, p) level of theory.

	Forward reaction E_a		Reverse reaction E_a	
T (K)	CVT	CVT / SCT	CVT	CVT / SCT
200	22.1	13.5	11.2	2.6
250	21.9	15.4	11.1	4.6
300	21.7	17.1	11.0	6.4
350	21.6	18.3	10.9	7.6
400	21.5	18.9	11.0	8.4
450	21.5	19.4	10.9	8.8
500	21.4	19.8	10.9	9.3
600	21.4	20.3	11.0	9.8
800	21.5	20.7	11.1	10.4

For the formamide–water system, it proceeds via a concerted two-stage mechanism that involves a small compression of the NCO bond angle before changes in bond lengths occur. Water acts as a bridge between the donor and acceptor sites as results yield smaller compression of the NCO angle and, consequently, lowers the barrier from the gas phase by a factor of 2.1 at the BH&H-LYP level. The ZPE motion and tunneling significantly enhances the proton-transfer rate. In particular, the BH&H-LYP CVT/SCT activation energy at 300 K is only 17.1 kcal/mol, which is 7.0 kcal/mol below the classical. Of this, 3.4 kcal/mol is from the ZPE motion and 3.6 kcal/mol from quantum mechanical tunneling.

We are especially encouraged to see excellent agreement between the DFT and MP2 structural and frequency data. Particularly for the formam ide–water structure, all methods are in excellent agreement with the expensive QCISD method. The classical and zero-point energy barriers to tautomerization for both the gas-phase and water-assisted cases are best predicted by the BH&H-LYP method when compared to the more accurate CISD(FULL) and QCISD methods. When taking into consideration both accuracy and cost, the BH&H-LYP method is the better method compared to the B-LYP, B3-LYP, and MP2 methods for rate calculations.

ACKNOWLEDGMENTS

This work was supported by the University of Utah and the National Science Foundation through

an NSF Young Investigator Award to T. N. T. and NSF Grant No. 9116286 to J. S.

References

1. S. A. Aziz and C. O. Knowles, Nature **242,** 418 (1973).
2. R. W. Beeman and F. Matsumura, Nature **242,** 274 (1973).
3. T. L. Johnson and C. O. Knowles, Gen. Pharm **14,** 591 (1983).
4. D. N. Silverman and S. Lindslog, Acc. Chem. Res. **21,** 30 (1988).
5. P. G. Jasien and W. J. Stevens, J. Chem. Phys. **84,** 3271 (1986).
6. R. L. Bell and T. N. Truong, J. Chem. Phys. **101,** 10442 (1994).
7. T. Oie, G. H. Loew, S. K. Burt, J. S. Binkley, and R. D. MacElroy, J. Am. Chem. Soc. **104,** 6169 (1982).
8. T. Oie, G. H. Loew, S. K. Burt, and R. D. MacElroy, J. Am. Chem. Soc. **105,** 2221 (1983).
9. T. Oie, G. H. Loew, S. K. Burt, and R. D. MacElroy, J. Am. Chem. Soc. **106,** 8007 (1984).
10. T. Ottersen and H. H. Jensen, J. Mol. Struct. **26,** 375 (1975).
11. F. J. Lovas, R. P. Suenram, G. T. Fraser, C. W. Gillies, and J. Zozom, J. Chem. Phys. **88,** 722 (1988).
12. M. Bodansky, *Peptide Chemistry*: *A Practical Textbook* (Springer-Verlag, Berlin, 1988).
13. M. Bodansky, *Principle of Peptide Synthesis*, 2nd ed. (Springer-Verlag, Berlin, 1993).
14. X. C. Wang, J. Nichols, M. Feyereisen, M. Gutowski, J. Boatz, A. D. J. Haymet, and J. Simons, J. Phys. Chem. **95,** 10419 (1991).
15. J. F. Hinton and R. D. Harpool, J. Am. Chem. Soc. **99,** 349 (1977).
16. G. Alagona, A. Pullman, E. Scrocco, and J. Tomasi, J. Peptide Protein Res. **5,** 251 (1973).
17. A. Pullman, H. Berthod, C. Giessner-Pretter, J. F. Hinton, and D. Harpool, J. Am. Chem. Soc. **100,** 3991 (1978).
18. T. J. Zielinski, R. A. Poirier, M. R. Peterson, and I. G. Csizmadia, J. Comput. Chem. **4,** 419 (1983).
19. M. Nagaoka, Y. Okuno, and T. Yamabe, J. Am. Chem. Soc. **113,** 769 (1991).
20. A. Engdahl, B. Nelander, and P. O. Åstrand, J. Chem. Phys. **99,** 4894 (1993).
21. J. D. Pranata and D. Geraldine, J. Phys. Chem. **99,** 14340 (1995).
22. Q. Zhang, R. L. Bell, and T. N. Truong, J. Phys. Chem. **99,** 592 (1995).
23. T. N. Truong, W. T. Duncan, and R. L. Bell, in *Chemical Applications of Density-Functional Theory*, B. B. Laird, R. B. Ross, and T. Ziegler, Eds. (American Chemical Society, Washington, DC, 1996), pp. 85–104.
24. T. Yamabe, K. Yamashita, M. Kaminoyama, M. Koizumi, A. Tachibana, and K. Fukui, J. Phys. Chem. **88,** 1459 (1984).
25. T. N. Truong and J. A. Mccammon, J. Am. Chem. Soc. **113,** 7504 (1991).
26. D. G. Truhlar, in *The Reaction Path in Chemistry*: *Current Approaches and Perspectives*, D. Heidrich, Ed. (Kluwer, Dordrecht, Netherlands, 1995), pp. 229–255.
27. D. G. Truhlar and B. C. Garrett, Acc. Chem. Res. **13,** 440 (1980); *Ibid*. J. Am. Chem. Soc., **101,** 4534 (1979).
28. D. G. Truhlar, A. D. Isaacson, and B. C. Garrett, in *Theory of Chemical Reaction Dynamics*, M. Baer, Ed. (CRC Press, Boca Raton, FL, 1985), pp. 65–137.
29. S. C. Tucker and D. G. Truhlar, in *New Theoretical Concepts for Understanding Organic Reactions*, J. Bertran and I. G. Csizmadia, Eds. (Kluwer, Dordrecht, Netherlands, 1989), pp. 291–346.
30. E. Wigner, Z. Phys. Chem. B **19,** 203 (1932).
31. T. N. Truong and D. G. Truhlar, J. Chem. Phys. **93,** 1761 (1990).
32. D. G. Truhlar, A. D. Isaacson, R. T. Skodje, and B. C. Garrett, J. Phys. Chem. **86,** 2252 (1982).
33. M. J. Frisch, G. W. Trucks, M. Head-Gordon, P. M. W. Gill, M. W. Wong, J. B. Foresman, B. G. Johnson, H. B. Schlegel, M. A. Robb, E. S. Replogle, R. Gomperts, J. L. Andres, K. Raghavachari, J. S. Binkley, C. Gonzalez, R. L. Martin , D. J. Fox, D. J. DeFrees, J. Baker, J. J. P. Stewart, and J. A. Pople, *Gaussian 92/DFT* (Gaussian Inc., Pittsburgh, PA, 1992).
34. M. J. Frisch, G. W. Trucks, H. B. Schlegel, P. M. W. Gill, B. G. Johnson, M. A. Robb, J. R. Cheeseman, T. Keith, G. A. Petersson, J. A. Montgomery, K. Raghavachari, M. A. Al-Laham, V. G. Zakrzewski, J. V. Ortiz, J. B. Foresman, J. Cioslowski, B. B. Stefanov, A. Nanayakkara, M. Challacombe, C. Y. Peng, P. Y. Ayala, W. Chen, M. W. Wong, J. L. Andres, E. S. Replogle, R. Gomperts, R. L. Martin, D. J. Fox, J. S. Binkley, D. J. Defrees, J. Baker, J. P. Stewart, M. Head-Gordon, C. Gonzalez, and J. A. Pople, *Gaussian 94*, *Revision B.1* (Gaussian Inc., Pittsburgh, PA, 1995).
35. W. T. Duncan and T. N. Truong, to be published.
36. T. N. Truong and W. T. Duncan, *TheRate*; more information is available at http://www.chem.utah.edu/mercury/TheRate/TheRate.html.
37. Y. Sugawara, Y. Hamada, and M. Tsuboi, Bull. Chem. Soc. Jpn. **56,** 1045 (1983).
38. T. Dunning, J. Chem. Phys. **90,** 1007 (1989).
39. T. N. Truong and W. Duncan, J. Chem. Phys. **101,** 7408 (1994).